Entrainment in stratified environments — an interface-based approach

Dominik Krug[1], Maarten van Reeuwijk[2], Markus Holzner[3] and Ivan Marusic[1]

[1] Department of Mechanical Engineering, The University of Melbourne,
dominik.krug@unimelb.edu.au
[2] Department of Civil and Environmental Engineering, Imperial College London
[3] Institute of Environmental Engineering, ETH Zürich

Abstract

In this study, we focus on understanding stratification effects on the entrainment process in gravity currents via a multi-scale approach based on the turbulent/non-turbulent interface (TNTI). We find that a large part of the reduction of the entrainment parameter in the presence of a stable stratification can be explained through a reduction of the surface area of the TNTI. An analysis of the fractal geometry of the TNTI reveals that the decrease of the surface area with increasing stable stratification is predominantly due to a reduced effective fractal dimension.

1 Introduction

Turbulent entrainment across stably stratified interfaces is widespread in many geophysical and engineering applications. In this paper, we focus on the case of gravity currents which is relevant to a wide range of flow scenarios (Simpson, 1999). It has long been known that in this kind of flow entrainment decreases with increasing Richardson number Ri, i.e. with increasing relative strength of the stable stratification compared to the destabilizing shear (Ellison and Turner, 1959). Instead of providing a parametrization of entrainment in terms of bulk quantities, our goal here is to investigate the multi-scale processes that give rise to turbulent entrainment.

It is widely observed that sharp and strongly contorted interfaces separate turbulent and non-turbulent regions in partly turbulent flows such as jets, wakes, boundary layers and many more (Corrsin and Kistler, 1954; Da Silva et al., 2014). In the present investigation, we study entrainment in terms of the volume flux through this turbulent/non-turbulent interface (TNTI). Defining the TNTI using an appropriate threshold on enstrophy ω^2, where ω denotes the norm of the vorticity vector, the local entrainment velocity can be defined as the motion of the TNTI relative to the fluid, which can be computed from $v_n \equiv -|\nabla \omega^2|^{-1} D\omega^2/Dt$ (Holzner and Lüthi, 2011). The entrained volume flux is then given by the surface integral $Q_\omega \equiv \int_{A_\eta} v_n dA = \langle v_n \rangle A_\eta$, where A_η is the surface area of the TNTI and $\langle \cdot \rangle$ denotes an average over A_η. In Krug et al. (2015), we showed that the bulk entrainment coefficient $E \equiv u_e/u_T$, where u_e is the global entrainment velocity and u_T the top-hat velocity, can equivalently be obtained via a TNTI-based approach from

$$E_I = -\frac{v_n}{u_T} \frac{A_\eta}{A_0} \frac{h}{h_\omega}. \tag{1}$$

Here, h is the top-hat thickness, h_ω the mean TNTI position off the wall and the factor h/h_ω represents a self-similarity correction of the entrained fluxes. Note also that the subscript I only serves to identify the way E was computed and it has been verified that $E = E_I$ by Krug et al. (2015) and van Reeuwijk et al. (2016). Based on this result, it is
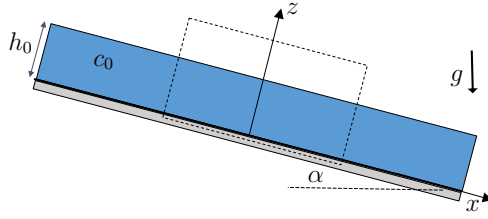
Figure 1: Simulation setup, c_0 is the initial distribution of the scalar c, g denotes the gravitational acceleration.

possible to link changes of E to changes of the individual factors on the right hand side of (1).

It is now widely accepted that the local spreading of the TNTI is a small-scale process with v_n of the order of the Kolmogorov velocity. Further, Krug et al. (2015) (in an experiment) and more recently van Reeuwijk et al. (2016) (based on simulations) showed that an additional contribution to v_n by the baroclinic torque remains negligibly small. These results suggest that A_η is the driving parameter in reducing the entrainment rate in the presence of stratification. We will test this proposition in this paper via direct numerical simulations (DNS) and focus on buoyancy effects on A_η.

2 Simulations

We perform simulations of a temporal version of the Boussinesq gravity current problem with periodic boundary conditions in the streamwise direction. The simulation setup is sketched in figure 1 and a more complete description of the simulations is presented in van Reeuwijk et al. (2016). In this paper, we present results from three different simulations, one of which is a wall jet (WJ) with no buoyancy effects and the remaining two are gravity currents (labelled GC1 and GC2) with different stratification levels. In table 1, we list details for these runs with the bulk Reynolds number defined as $Re = u_T h/\nu$ and the Richardson number $Ri = -\gamma \cos \alpha g c_T h/(u_T)^2$. Initial values of all quantities are marked with subscript 0. Further, α denotes the inclination angle and g the gravitational acceleration; c is the scalar concentration and γ a coefficient for the linear change of density due to the presence of the scalar c. Top-hat quantities (marked with subscript T) are defined by

$$u_T h = \int_0^\infty \overline{u}\,dz, \qquad u_T^2 h = \int_0^\infty \overline{u}^2\,dz, \qquad c_T h = \int_0^\infty \overline{c}\,dz, \qquad (2)$$

where u is the streamwise velocity and the overline indicates an average over a wall-parallel plane.

Table 1: Dimensionless parameters of the simulations.

Sim.	$N_x N_y N_z$	$L_x L_y L_z / h_0^3$	Re_0	Ri_0	E	S/L_x
WJ	$1536^2 \times 1152$	$20^2 \times 10$	3700	0	0.088	1.81
GC1	$1536^2 \times 1152$	$20^2 \times 10$	3700	0.04	0.030	1.41
GC2	$1536^2 \times 1152$	$20^2 \times 10$	3700	0.11	0.016	1.25

The temporal evolution of some characteristic quantities for the three simulations is presented in figure 2. It is clearly observed that increasing Ri_0, leads to a slower growth
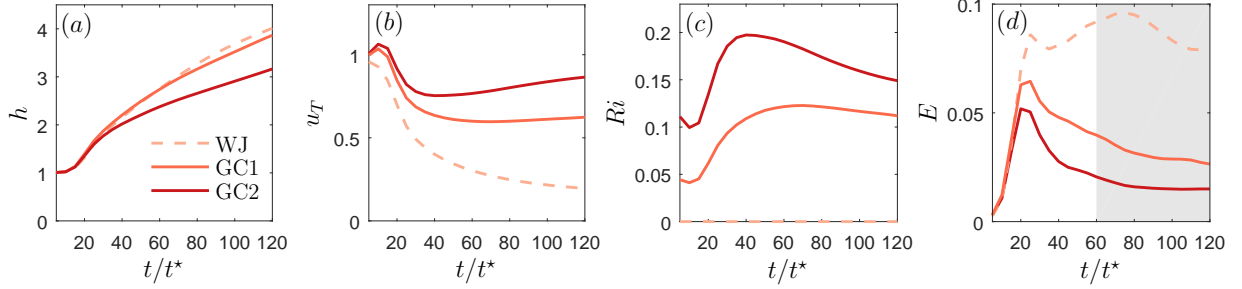
Figure 2: Temporal evolution of characteristic quantities for wall jet (WJ) and gravity currents (GC1 and GC2). (a) top-hat thickness h. (b) top-hat velocity u_T. (c) Richardson number Ri. (d) entrainment coefficient E. The grey shaded area in (d) indicates the averaging time for the result reported in table 1. Legend in (a) applies to all panels.
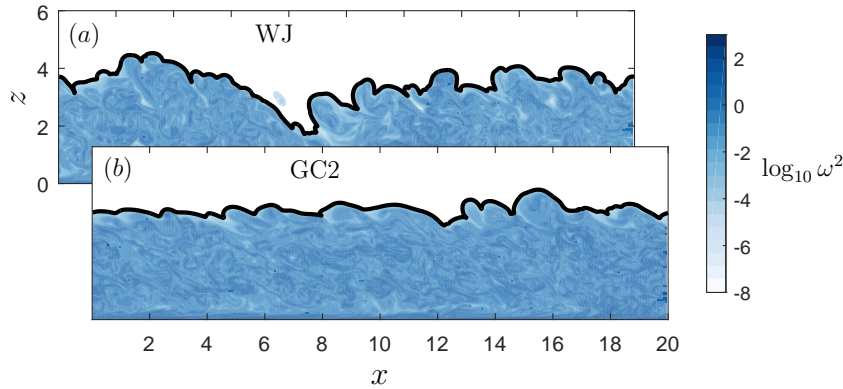

Figure 3: Snapshots of the enstrophy distribution in (a) WJ at $t/t^* = 60$ and (b) GC2 at $t/t^* = 90$ with the times selected such that $h = 2.75$ in both flows. Black solid lines indicate the position of the TNTI based on a threshold value $\omega_{thr}^2 = 3 \cdot 10^{-5}(u_0/h_0)^2$.

rate of h (cf. figure 2a), higher values of u_T (cf. figure 2b) and somewhat higher Ri in figure 2c once the flow has reached an approximate equilibrium around $60 t/t^*$, where the reference time-scale $t^* = h_0/u_{T0}$. Most importantly, we find that the entrainment coefficient computed from $E = u_T^{-1} dh/dt$ strongly depends on the stratification level and decreases with increasing Ri, a result that conforms with previous research (Ellison and Turner, 1959).

3   Stratification effects on TNTI area

Figure 3 show snapshots of fields of enstrophy ω^2 for the unstratified WJ (figure 3a) and the gravity current GC2 (figure 3b). It is common practice to define the TNTI based on an threshold on enstrophy (Da Silva et al., 2014). For the purpose of this study, we use a threshold value $\omega_{thr}^2 = 3 \cdot 10^{-5}(u_0/h_0)^2$ in all simulations. A detailed study of threshold dependence is beyond the scope of this work but we note that different choices of ω_{thr}^2 have no impact on our principal conclusions here for a wide range of thresholds. For a detailed investigation of the threshold-dependence of the TNTI position we refer to van Reeuwijk et al. (2016), where the effect of varying the threshold over several orders of magnitude was studied.

From figure 3 it is immediately obvious that the TNTI, which is indicated by the black line, in the GC2 snapshot is considerably less contorted than the one from the WJ simulation. To quantify this observation, we measure the length S of the interface as a 2D surrogate
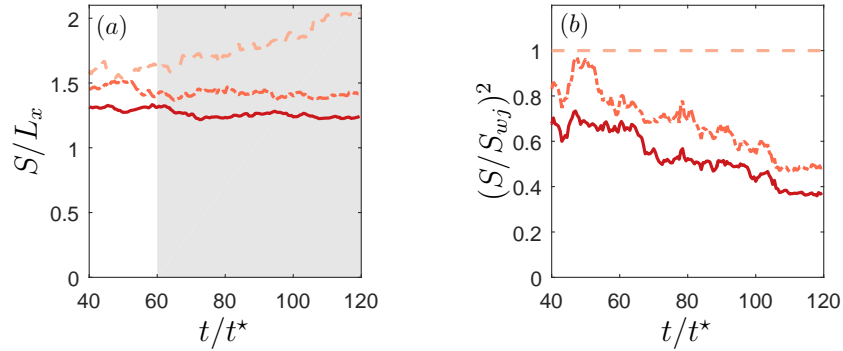
Figure 4: (a) Length S as a function of time for the three flow cases. (b) Squared ratio of the respective value of S to the one obtained in the GC simulation (represents estimate of the relative reduction of TNTI surface area). The legend in 2a applies; shaded area in (a) indicates averaging time for value listed in table 1.

for A_η and report the ratio S/L_x for all three flow cases investigated in figure 4a. Here and in the following, results are presented as averages over 5 wall-normal/streamwise slices of the flowfield. As expected, the values for the stratified flows are considerably lower with GC2 only reaching $S/L_x \approx 1.2$ while the result for the WJ is close to 2. In order to be able to gauge the reduction of E associated with the reduced surface area of the TNTI in the stratified flows, we plot $(S/S_{wj})^2$ in figure 4b. The reason for taking the square is that the surface area appears in (1) while S has the dimension of length only. Using S^2 is an approximation in the sense that it assumes that the level of contortion in the spanwise direction is equal to the one measured in the slices oriented in the streamwise direction. The values of $(S/S_{wj})^2$ are significantly lower than 1 throughout for both GC1 and GC2. Towards the end of the simulations $(S/S_{wj})^2 \approx 0.5$ which is comparable to, albeit slightly less, than the reduction in E observed in figure 2d, confirming that the reduction of the surface area of the TNTI plays a dominant role in reducing the entrainment rate across stably stratified interfaces.

4 Fractal scaling

In unstratified environments it was found that the surface area of the TNTI exhibits fractal scaling such that $A_\eta \propto (l_i/l_o)^{-\beta}$ where l_i and l_i are the inner and outer cutoff of the scaling range, respectively and β is the scaling exponent which is equal to $1/3$ in the unstratified case (Sreenivasan et al., 1989). In order to be able to investigate potential changes to this fractal scaling due to buoyancy, we evaluate the TNTI contortions at different scales by applying a filter. As a first step of the filtering approach adopted here, we transform the enstropy field into a binary field which is 1 where $\omega^2 > \omega_{thr}^2$ and 0 elsewhere. This binary field is subsequently filtered using a box filter of size λ. The filtered TNTI is then obtained from the isocontour at a value of 0.5 in the filtered field. An illustration of this procedure is provided in figure 5a, where the unfiltered binary field is shown on the top and the filter seize increases in the two panels below. The main advantage of filtering the binary field instead of the enstrophy field directly is that when using the binary field, the average interface position is (almost) invariant to the filtering. The length of the TNTI in the filtered fields is plotted as symbols in figure 5b. For very small λ it remains constant at the unfiltered value indicating that no contortions exist at these scales. As λ is increased beyond the inner cutoff l_i, more and more convolutions of the TNTI are removed and $S(\lambda)$ decreases. For a fractal geometry this decrease will
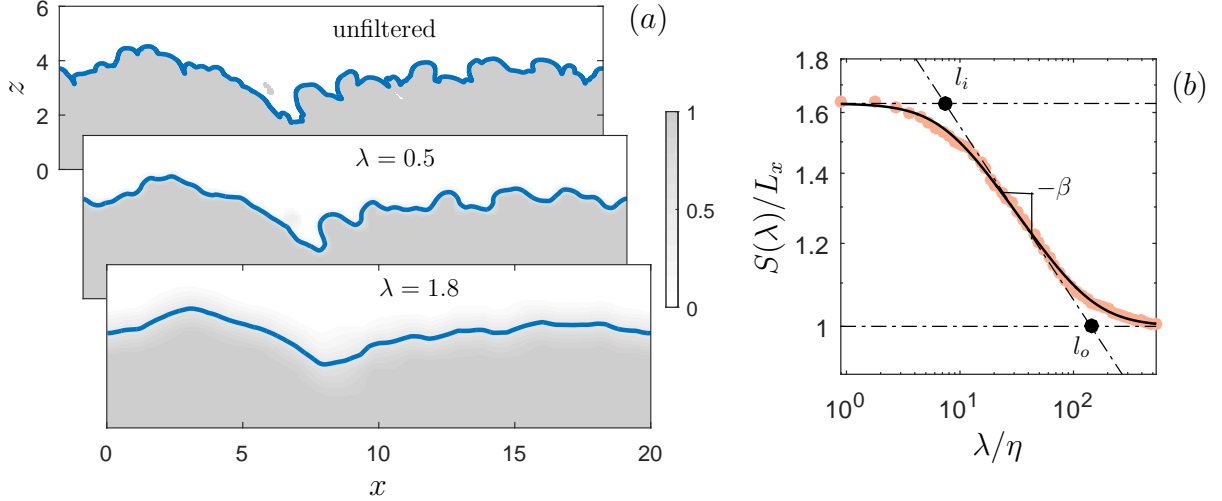
Figure 5: (a) Illustration of the filtering procedure applied to the enstrophy snapshot shown in figure 3a. The blue line represents the TNTI at the respective filter scale. (b) Interface length S (round symbols) as a function of filterscale λ for the snapshot shown in (a). Shown as black solid line is the corresponding fit according to 3.

be proportional to $\lambda^{-\beta}$. At even larger filter sizes the curve in figure 5b levels off at $S(\lambda)/L_x = 1$, which is indicative of the fact that at this point, i.e. for λ larger than the outer cutoff l_0, even oscillations with the largest wavelengths present are removed and the filtered interface approaches a straight line. Following Thiesset et al. (2016), we employ a fit of the form

$$\frac{S(\lambda)}{L_x} = \left(\frac{l_o}{l_i}\right)^{\beta} \left[\frac{1 + (\lambda/l_o)^2}{1 + (\lambda/l_i)^2}\right]^{\beta/2} \tag{3}$$

to determine the values of l_i, l_o and β as unambiguously as possible from $S(\lambda)$. As figure 5b shows, this functional form allows to represent the data very accurately when using l_i, l_o and β as free parameters of the fit.

The results from applying the fit to the three different flows and at different times are displayed in figure 6. The inner cutoff is determined by the scale of the smallest eddies which are characterized by the Kolmogorov scale $\eta = (\nu/\varepsilon)^{1/4}$, where the rate of turbulent dissipation ε is taken as the average over the turbulent zone excluding the near-wall region $z < 0.3h$. According to figure 6a, $l_i \approx 10\eta$ in all flows conforming with findings for the TNTI in a turbulent boundary layer (de Silva et al., 2013). The outer cutoff in figure 6b is seen to collapse reasonably well when rescaled with the respective value of h and beyond $t/t^* = 60$ we find that $l_o/h \approx 0.6h$. Presumably due to the limited Reynolds number of the simulations, the slope for the WJ in figure 6c does not quite reach the theoretically predicted value of $1/3$. However, there is a distinct tendency of β to decrease with increasing stratification levels. Specifically , we find that $\beta \approx 0.12$ for GC1 and $\beta = 0.08$ for GC2 with no apparent changes as the flows evolve in time, while the WJ reaches $\beta \approx 0.25$ at later times.

5 Conclusion

Using direct numerical simulations of gravity currents with different initial Richardson numbers, the effect of stable stratification on the entrainment process was studied in a
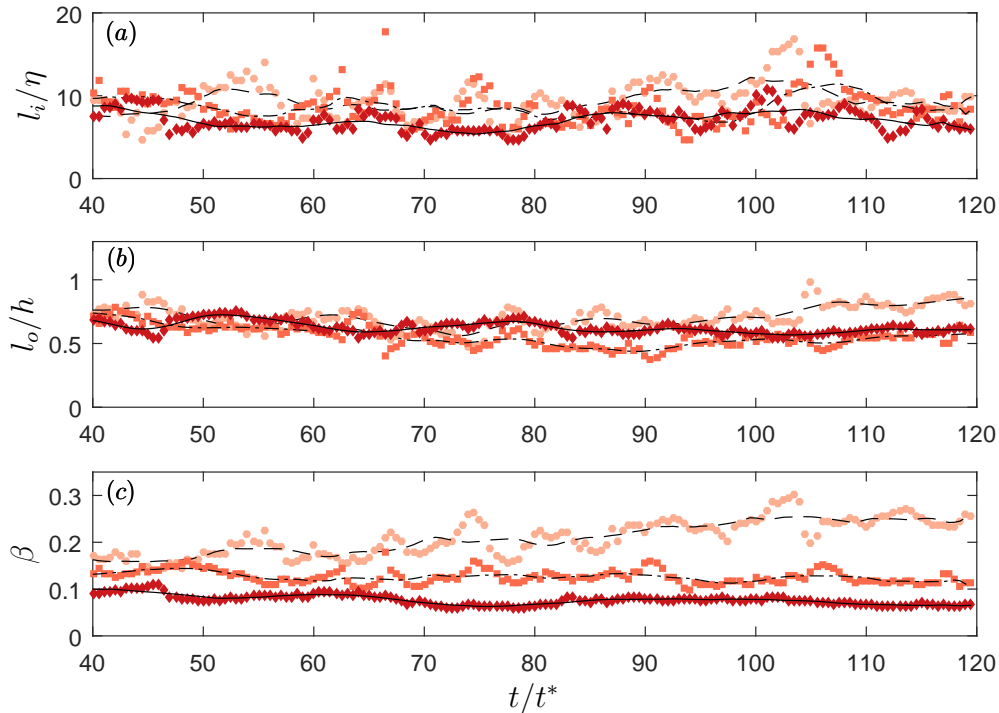
Figure 6: Results from applying the fit according to (3) for WJ (circles, dashed line), GC1(squares, dashed-dotted) and GC2(diamonds,solid). (a) inner cutoff l_i. (b) outer cutoff l_o. (c) slope β. Black lines indicate the moving average over a span of 20 points ($\approx 10t/t^*$).

multi-scale framework. The focus here is on buoyancy induced changes to the geometry of the turbulent/non-turbulent interface (TNTI). We find that the surface area of the TNTI is significantly reduced by the presence of a stable stratification and that this reduction plays an important role in reducing the effective entrainment rate as previously conjectured in Krug et al. (2015) and van Reeuwijk et al. (2016). An analysis of the fractal scaling of the interface revealed that for the flows considered, the main effect of the stratification is to reduce the slope in the fractal scaling regime. Effects on the outer cutoff of the fractal scaling range appear to be well represented by changes to the top-hat thickness h, while the inner cutoff remains on the order of the Kologorov lengthscale with buoyancy effects restricted to setting the overall turbulence levels in the flow.

References

Corrsin, S. and Kistler, A. (1954). The free-stream boundaries of turbulent flows. *NACA*, TN-3133, TR-1244:1033–1064.

Da Silva, C. B., Hunt, J. C. R., Eames, I., and Westerweel, J. (2014). Interfacial layers between regions of different turbulence intensity. *Annu. Rev. Fluid Mech.*, 46:567–590.

de Silva, C. M., Philip, J., Chauhan, K., Meneveau, C., and Marusic, I. (2013). Multi-scale Geometry and Scaling of the Turbulent-Nonturbulent Interface in High Reynolds Number Boundary Layers. *Phys. Rev. Lett.*, 111:044501.

Ellison, T. H. and Turner, J. S. (1959). Turbulent entrainment in stratified flows. *J. Fluid Mech.*, 6(03):423–448.

Holzner, M. and Lüthi, B. (2011). Laminar Superlayer at the Turbulence Boundary. *Phys. Rev. Lett.*, 106(13):134503.

Krug, D., Holzner, M., Lüthi, B., Wolf, M., Kinzelbach, W., and Tsinober, A. (2015). The turbulent/non-turbulent interface in an inclined dense gravity current. *J. Fluid Mech.*, 765:303–324.

Simpson, J. E. (1999). *Gravity Currents.* Cambridge University Press.

Sreenivasan, K. R., Ramshankar, R., and Meneveau, C. (1989). Mixing, entrainment and fractal dimensions of surfaces in turbulent flows. *Proc. R. Soc. A*, 421(1860):79–108.

Thiesset, F., Maurice, G., Halter, F., Mazellier, N., Chauveau, C., and Gökalp, I. (2016). Geometrical properties of turbulent premixed flames and other corrugated interfaces. *Phys. Rev. E*, 93(1):013116.

van Reeuwijk, M., Krug, D., and Holzner, M. (2016). Small-scale entrainment in gravity currents. *Environmental Fluid Mechanics*, submitted.